

Enhancement of optical transparency in Bi_2O_3 -modified $(\text{K}_{0.5}\text{Na}_{0.5})_{0.9}\text{Sr}_{0.1}\text{Nb}_{0.9}\text{Ti}_{0.1}\text{O}_3$ ceramics for electro-optic applications

Zhiyong Liu¹ · Huiqing Fan¹ · Biaolin Peng²

Received: 7 May 2015 / Accepted: 17 August 2015 / Published online: 25 August 2015
© Springer Science+Business Media New York 2015

Abstract Transparent relaxor ferroelectrics, $(\text{K}_{0.5}\text{Na}_{0.5})_{0.9}\text{Sr}_{0.1}\text{Nb}_{0.9}\text{Ti}_{0.1}\text{O}_3-x\%\text{Bi}_2\text{O}_3$ ($x = 0, 0.5, 1.0, 1.5,$ and 2 , abbreviated as KNSNT-10 x), were fabricated using a pressureless sintering method. With the modification of Bi_2O_3 , the crystal phase of KNSNT ceramics transformed from tetragonal to cubic-like symmetry, and dielectric behaviors became more relaxor like. These changes could reduce the light scattering arisen from birefringence and long-range ordering structure, thus enhancing the optical properties. For KNSNT-10 transparent ceramics, fingerprint morphological nanodomains were observed in the transmission electron microscope image, which made the ceramics sensitive to electric field. Therefore, a large effective linear electro-optic coefficient of 26.1 pm/V was obtained for the KNSNT-10 ceramics, and it is higher than the value (19.9 pm/V) for LiNbO_3 single crystal.

Introduction

High-quality optical materials with a large electro-optic (EO) response are highly desirable for various optical applications, such as light shutters, modulators, and color

filter devices [1–3]. LiNbO_3 single crystal is the industry benchmark of EO materials [4, 5]. However, the small available size, high cost, long growth time, and low EO response make it difficult for a wide range of applications. Compared with the LiNbO_3 single crystal, transparent ceramics have apparent advantages, e.g., ceramic ruggedness, easy fabrication, low fabrication cost, large available size, and stronger EO responses [1, 6].

Currently, lead-based transparent ceramics are widely studied [6–10], such as $(\text{Pb}_{1-x}\text{La}_x)(\text{Zr}_y\text{Ti}_{1-y})_{1-x/4}\text{O}_3$, $\text{Pb}(\text{Mg}_{1/3}\text{Nb}_{2/3})\text{O}_3\text{--PbTiO}_3$, and $\text{Pb}(\text{Zn}_{1/3}\text{Nb}_{2/3})\text{O}_3\text{--PbTiO}_3$ system. The lead-based materials have a major drawback, that is their high lead content (more than 60 wt%). In order to protect environment, there is a need of replacing the lead-based materials by environmental friendly lead-free materials. $\text{K}_{0.5}\text{Na}_{0.5}\text{NbO}_3$ is one of the most promising candidates for lead-free piezoelectric ceramics and has been studied extensively [11–17]. The sintering behaviors and piezoelectric properties of the ceramics can generally be enhanced by the addition of different ions or the formation of new solid solutions with other ferroelectrics, such as Li^+ , Bi^{3+} , Ta^{5+} , BaTiO_3 , and SrTiO_3 . However, there are few works to report on enhancing optical properties of the ceramics. The early paper with regard to $\text{K}_{0.5}\text{Na}_{0.5}\text{NbO}_3$ translucent ceramics was reported by Kosec et al. [17, 18]. Owing to the fine-grained and high-density microstructure, $0.8\text{K}_{0.5}\text{Na}_{0.5}\text{NbO}_3\text{--}0.2\text{SrTiO}_3$ ceramics with a pseudo-cubic perovskite structure became translucent; and their quadratic EO property also has been measured. Unfortunately, Curie temperature of the $0.8\text{K}_{0.5}\text{Na}_{0.5}\text{NbO}_3\text{--}0.2\text{SrTiO}_3$ (about 230 K) is below the room temperature, resulting in a weak ferroelectricity, so that the quadratic EO coefficient is one order of magnitude smaller than that of the commercial PLZT ceramics. Recently, Kwok et al. [19, 20] employed the hot isostatic

Electronic supplementary material The online version of this article (doi:10.1007/s10853-015-9360-y) contains supplementary material, which is available to authorized users.

✉ Huiqing Fan
hqfan3@163.com

¹ State Key Laboratory of Solidification Processing, School of Materials Science and Engineering, Northwestern Polytechnical University, Xi'an 710072, China

² Department of Applied Physics, The Hong Kong Polytechnic University, Kowloon, Hong Kong

pressing sintering technique to obtain transparent $(\text{K}_{0.5}\text{Na}_{0.5})_{1-x}\text{Li}_x\text{Nb}_{1-x}\text{Bi}_x\text{O}_3$ ceramics, which exhibited a high linear EO coefficient. These results indicate that the $\text{K}_{0.5}\text{Na}_{0.5}\text{NbO}_3$ lead-free material is a good candidate to replace the lead-based transparent ceramics.

The lead-free $(\text{K}_{0.5}\text{Na}_{0.5})_{0.9}\text{Sr}_{0.1}\text{Nb}_{0.9}\text{Ti}_{0.1}\text{O}_3$ solid solution exhibits proto-typical relaxor ferroelectric behavior and Curie temperature near 148 °C [21, 22]. In this work, we prepared transparent $(\text{K}_{0.5}\text{Na}_{0.5})_{0.9}\text{Sr}_{0.1}\text{Ti}_{0.1}\text{Nb}_{0.9}\text{O}_3-x\%\text{Bi}_2\text{O}_3$ EO ceramics, the effects of Bi_2O_3 on their microstructure, optical and electrical properties were investigated.

Experimental

Ferroelectric ceramics, $(\text{K}_{0.5}\text{Na}_{0.5})_{0.9}\text{Sr}_{0.1}\text{Nb}_{0.9}\text{Ti}_{0.1}\text{O}_3-x\%\text{Bi}_2\text{O}_3$ ($x = 0, 0.5, 1.0, 1.5$ and 2.0 , abbreviated as KNSNT-10 x), were prepared using the conventional solid-state reaction route. Stoichiometric raw oxides of K_2CO_3 , Na_2CO_3 , Nb_2O_5 , SrCO_3 , TiO_2 , and Bi_2O_3 (Sinopharm Chemical Reagent Co., Ltd, Shanghai, China) were mixed and then milled using a zirconia ball medium with ethanol for 12 h. After ball milling, the mixtures were dried and then calcined at 900 °C for 2 h. The precursor powders were ball milled for 24 h again, dried, and cold isostatically pressed into pellets at 300 MPa. The pressed pellets were sintered at 1200 °C for 2 h without any pressure. The obtained pellets with a diameter of 8 mm were finally polished (with 5 nm diamond paste) to a thickness of 0.5 mm for optical property measurements.

Optical transmittance of the KNSNT-10 x ceramics was measured in the range of 300–850 nm using an UV–Vis spectrophotometer (UV-2550, Shimadzu Co., Tokyo, Japan). Refractive index of the ceramics was measured at 633 nm using a prism coupler (Model 2010, Metricon, Pennington, NJ). Crystal structures of the ceramics were detected using X-ray diffraction (XRD; X’Pert PRO MPD, Philips, Eindhoven, The Netherlands) with $\text{Cu K}\alpha$ radiation at room temperature; and their microstructures (thermally etched surface performed at 1100 °C for 30 min) were obtained using a field emission scanning electron microscope (FE-SEM; JEOL-6700F, Japan Electron Co., Tokyo, Japan) operated at 20 kV. Electron diffraction patterns of the ceramics were observed using a transmission electron microscope (TEM; Tecnai F30, FEI, Hillsboro, OR) operated at 300 kV accelerating voltage. Raman scattering experiments were performed with an instrument (LabRAM HR800, Horiba JobinYvon, Lyon, France) in a backward scattering geometry (the exciting source was the 514.5 nm line from an argon ion laser). Weak-field dielectric responses of the ceramics were measured with a precision impedance analyzer (4294A, Agilent, Santa Clara, CA)

associated with a temperature controller (TP94, Linkam, Surrey, UK) over a temperature range of 293–773 K at a heating rate of 3 °C/min. Dependence of ferroelectric polarization (P) and longitudinally field-induced strain (S_{33}) were measured at 10 Hz, using a ferroelectric test unit (TF-2000, aix-ACCT, Aachen, Germany). Before EO test, the transparent ceramics were polarized under an electric field of 4 kV/mm for 30 min and then measured with a transverse geometry using a modified Sénarmont method [23]. The testing samples had a thickness of $t = 0.5$ mm, distance between electrodes of $d = 1.0$ mm, testing modulation frequency of $f = 1$ kHz, and a wavelength of $\lambda = 633$ nm.

Results and discussion

Figure 1 shows the photographs of the KNSNT-10 x ceramics with a thickness of 0.5 mm. It can be observed that the Bi_2O_3 content plays an important role in optical transparency. With increasing x content, the KNSNT-10 x ceramics are transformed from translucence to optical transparency. The enhancement in optical transparency is also observed in the optical transmittance spectra (Fig. 2). The optical transmittance T increases as the x content increases from 0 to 1.0 and then decreases rapidly with $x > 1.0$. For the $x = 1.0$ ceramic, a high optical transmittance of 51.5 % at the 633 nm wavelength is obtained. For transparent ceramic with a thickness t , transmittance T can be expressed as follows [24]:

$$T = (1 - R)^2 \exp(-\beta t), \quad R = \frac{(n - 1)^2}{(n + 1)^2}, \quad (1)$$

where R is the reflectivity, n is the refractive index of the ceramic, β is the scattering coefficient neglecting the absorption (generally extinction coefficient), and t is the sample thickness. For KNSNT-10 ceramic, the refractive index measured at 633 nm is 2.253, then about 29 % optical reflection loss could be calculated resulting from

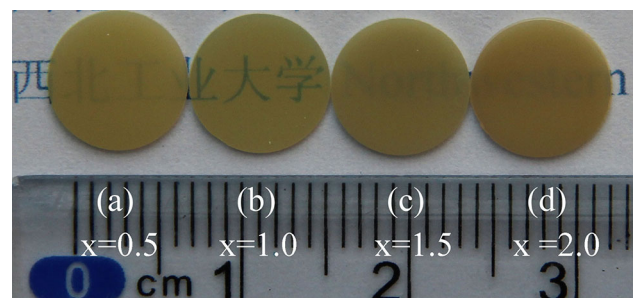


Fig. 1 Photographs of the KNSNT-10 x transparent ceramics

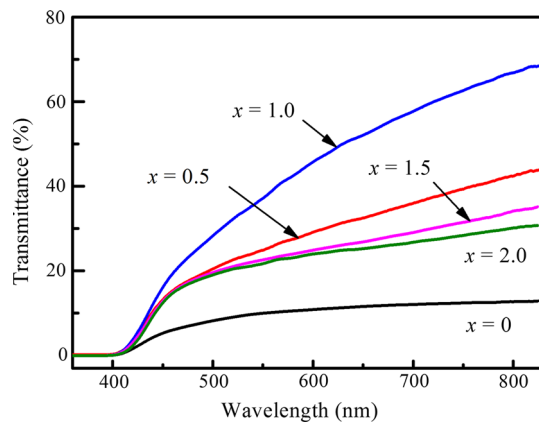


Fig. 2 Optical transmittance spectra of the KNSNT-10 x ceramics

twice air/ceramic interface reflection. If a proper antireflection coating is applied, the transmittance of the KNSNT-10 ceramic will be further improved to $\sim 81\%$.

EO effect describes the change in the refractive index Δn due to an applied electric field E . For polarized ferroelectric ceramics, we have [4]

$$\Delta n(E) = \frac{1}{2} n^3 r_c E. \quad (2)$$

Using a modified Sénarmont method [23], the effective EO coefficient can be calculated as

$$r_c = \frac{\lambda d}{\pi L n^3} \frac{\Gamma_m}{V_m}, \quad \Gamma_m = \frac{2\sqrt{2}V_{\text{rms}}}{V_{\text{p-p}}}, \quad (3)$$

where λ is the testing wavelength, n is the refractive index, r_c is the effective linear EO coefficient, d is the electrode spacing of the sample, L is the length along the light path, V_m is the peak-to-peak value of the applied ac electric field, and Γ_m is the phase shift degree. Besides, $V_{\text{p-p}}$ is the maximum voltage output of the ceramic without electric field; and V_{rms} is the maximum voltage output under an applied electric field. Figure 3a shows responded voltage of the photo-detection system as a function of analyzer angle of the $x = 1.0$ ceramic. V_0 is corresponding to the voltage output of the ceramic without electric field; and the $V_{\text{p-p}}$ value can be found from this curve. V_E is the voltage of the ceramic under an electric field, from which the V_{rms} can be obtained. Figure 3b shows phase shift (Γ_m) as a function of applied voltage V_m . It exhibits a remarkably linear behavior with the applied voltage. The effective EO coefficients can be determined from the slope of the curves associated with Eq. (3). A summary of r_c for the KNSNT-10 x ceramics is presented in Table 1. It can be found that the $x = 1.0$ transparent ceramic has an EO coefficient of 26.1 pm/V, which is higher than that of single crystal LiNbO₃ (19.9 pm/V) [4]. Besides, the EO coefficients are

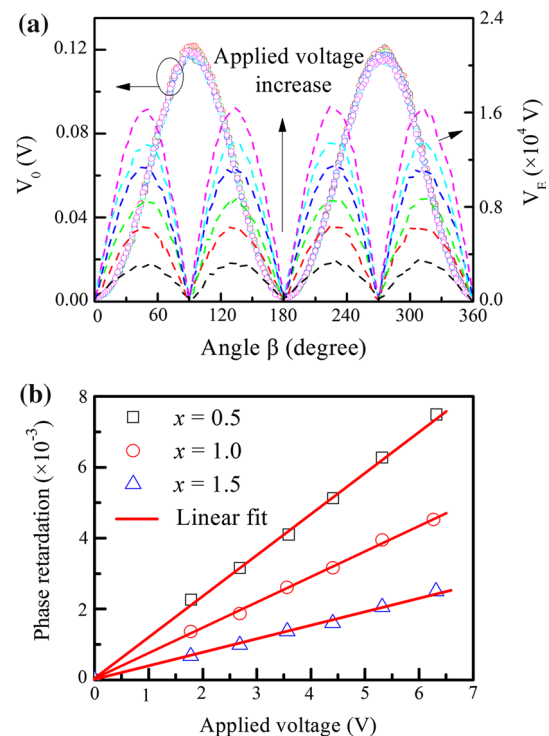


Fig. 3 **a** Responding voltage of the photo-detection system as a function of analyzer angle for the $x = 1.0$ ceramic, **b** phase retardations as a function of ac applied field for the KNSNT-10 x ceramics

41.8 and 14.9 pm/V for the $x = 0.5$ and $x = 1.5$, respectively.

Figure 4 shows thermally etched surface micrographs of the KNSNT-10 x ceramics, along with the respective average grain size distribution diagrams. Bi₂O₃ has an obvious effect on the microstructure of the ceramics, especially the grain size (Table 1). The $x = 1.0$ ceramic consists of faceted and cube-shaped grains, with an average grain size of $0.21 \pm 0.04 \mu\text{m}$ (Fig. 4c). For $x = 2.0$, the microstructure becomes loose and the grain size is decreased to $0.16 \pm 0.03 \mu\text{m}$ (Fig. 4d). It can be suggested that the addition of Bi₂O₃ is effective in suppressing grain growth. The similar phenomenon has also been observed in other Bi-doped KNN systems, such as BiScO₃–(K_{0.5}Na_{0.5})NbO₃ [13], BiFeO₃–(Na_{0.515}K_{0.485})_{0.95}Nb_{0.8}Ta_{0.2}O₃ [16], and (Bi_{0.5}Na_{0.5})TiO₃–(K_{0.5}Na_{0.5})NbO₃ [25] ceramics. To understand the effect of Bi₂O₃ on the microstructure of KNSNT-10 x ceramics, EDS mapping spectra of each element in KNSNT-10 ceramic are shown in Fig. S1 (see electronic supplementary material). All of the elements are homogeneously distributed through the ceramic. It has been reported that the addition of Bi₂O₃ not only concentrated in grain boundaries to inhibit the grain growth during sintering process, but also diffused into the lattice by replacing A-site ions to compensate sintering loss of

Table 1 Transmittance, linear EO coefficient r_c at 633 nm, and average grain size for the KNSNT-10x ceramics

x	0	0.5	1.0	1.5	2.0
Transmittance (%)	11.4	32.3	51.5	27.6	25.7
r_c (pm/V)	–	41.8	26.1	14.9	–
Average grain size (μm)	0.32 ± 0.07	0.24 ± 0.05	0.21 ± 0.04	0.18 ± 0.04	0.16 ± 0.03

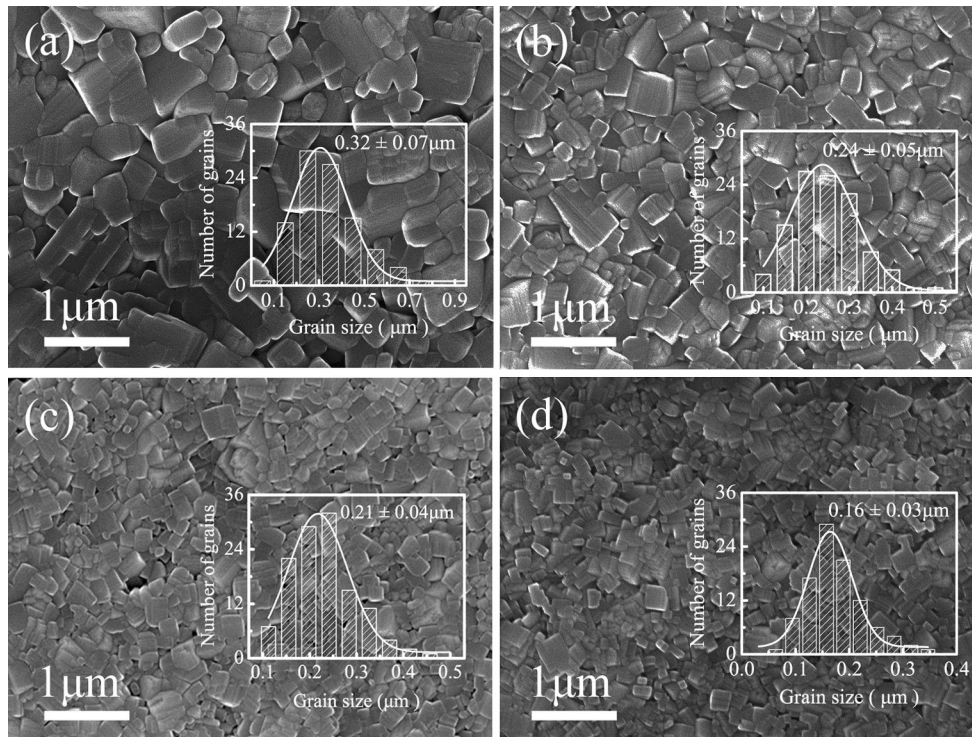


Fig. 4 SEM micrographs of thermally etched surfaces of the KNSNT-10x ceramics. **a** $x = 0$, **b** $x = 0.5$, **c** $x = 1.0$, and **d** $x = 2.0$. The insets show the grain size distributions

alkaline elements [26, 27]. This induces a homogeneous distribution of Bi ions.

From the results of alumina and yttrium aluminum garnet transparency ceramics [24, 28, 29], grain size, grain boundary, and pores are generally considered as the main factors affecting the transmittance of ceramics, while optical scattering by pores in ceramics should be considered as the main factor when the crystal structure is isotropic. According to Eq. (1), the scattering coefficient β , assuming single scattering spherical pores, can be expressed as [29]

$$\beta = \frac{p}{\frac{4}{3}\pi r^3} C_s, \tag{4}$$

where p is the porosity volume fraction, r is the pore radius, and C_s is the scattering cross section of the spherical pores. Pores can be frequently observed with a diameter of near 1 μm (Fig. 5a). As a result, the transmittance of the $x = 0$ ceramic is as low as 11.4 % (Table 1). In comparison, the

$x = 1.0$ ceramic shows a high optical transmittance with a fully dense and poreless microstructure in the fracture morphology. Besides, fracture surface of the $x = 1.0$ ceramic looks remarkably different. This also indicates that excess Bi_2O_3 addition may influence the mass transportation during the sintering and thus obviously induce densification of the ceramics as well as suppress the grain growth process [27].

XRD patterns of the KNSNT-10x ceramics are displayed in Fig. 6a. All of the ceramics possess a single perovskite structure. KNN shows orthorhombic symmetry, and the KNSNT($x = 0$) is tetragonal at room temperature [21, 22]. Notably, the addition of Bi_2O_3 caused the two peaks to merge into a sharp peak (Fig. 6b), suggesting that they may transform into another phase with very similar lattice constants, e.g., pseudo-cubic phase. Similar results have been observed in other KNN-based ceramics, such as Bi-modified KNN [20], KNN– SrTiO_3 [22], and KNN–($\text{Bi}_{0.5}\text{Na}_{0.5}$) TiO_3 [25]. In addition, Bi^{3+} (0.138 nm,

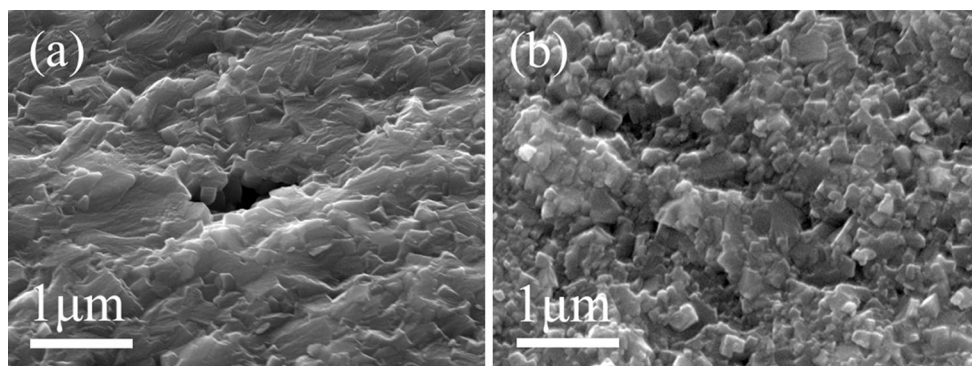


Fig. 5 SEM micrographs of fracture surfaces of the KNSNT-10 x ceramics. **a** $x = 0$ and **b** $x = 1.0$

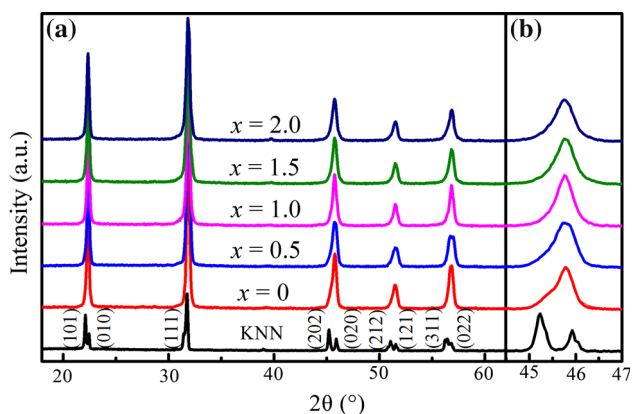


Fig. 6 XRD patterns of the KNSNT-10 x ceramics

CN = 12) is close to K^+ (0.164 nm, CN = 12) and Na^+ (0.138 nm, CN = 12). This suggests that Bi^{3+} ions can diffuse into A-site of the KNSNT lattices to compensate the sintering loss of alkaline elements [13, 30].

Figure 7 demonstrates temperature dependences of dielectric permittivity and dielectric loss ($\tan \delta$) of the KNSNT-10 x ceramics in the frequency range from 1 kHz to 1 MHz. KNN is a classical ferroelectric with two transition peaks: one is associated with the cubic-to-tetragonal phase transition at 428 °C and the other with the tetragonal-to-orthorhombic phase transition at 206 °C (Fig. 7a). With the addition of Bi_2O_3 , the ceramics exhibit a broadened cubic–tetragonal transition peak, which shifts to low temperature. In addition, the observed ϵ' decreases from 1583 to 828 at 10 kHz and 300 K as the content of Bi_2O_3 is increased from 0 to 2.0 (Table 2). Also, the temperatures (T_m) of the maximum dielectric permittivity and the corresponding peak values (ϵ'_m) at 10 kHz are decreased (Table 2). This result also indicates that Bi ions have diffused into the A-site of KNSNT ceramics. For the modified ceramics, an obvious diffuse phase transition can be observed, and the ϵ' decreases with increasing frequency, which is a typical characteristic for relaxor ferroelectrics.

For relaxor ferroelectrics, the reciprocity of the dielectric permittivity and temperature follow the Uchino and Nomura function, a modified Curie–Weiss law [31],

$$\frac{1}{\epsilon'} - \frac{1}{\epsilon'_m} = \frac{(T - T_m)^\gamma}{C}, \quad (5)$$

where C is Curie constant and γ is the diffusion coefficient of value ranging from one (a normal ferroelectric) to two (an ideal relaxor ferroelectric). Figure 8 shows $\ln(1/\epsilon' - 1/\epsilon'_m)$ as a function of $\ln(T - T_m)$ at 10 kHz for the KNN, $x = 0, 1.0$, and 2.0, respectively. By least-squares fitting the experimental data according to the modified Curie–Weiss law, γ is determined, with results listed in Table 2. It can be found that the maximum value of γ is 2.0 for $x = 1.0$. Correspondingly, the $x = 1.0$ ceramic exhibits a much broader diffuse phase transition (Fig. 7c), suggesting that the ceramic is more relaxor like and contains more polar nanoregions [32, 33]. However, for ceramics with $x > 1.0$, the diffusion coefficient γ is decreased. This may be partly due to the appearance of electronic conduction at high temperatures (the $\tan \delta$ shown in Fig. 7d).

To further reveal the relaxor behaviors of the KNSNT-10 x ceramics, Fig. 9a shows Raman spectra of the ceramics at room temperature. The main vibration modes (ν_1 – ν_5) are associated with the NbO_6 octahedra. The peaks at $<160 \text{ cm}^{-1}$ can be assigned to the K^+/Na^+ translation and rotations of the NbO_6 octahedra [21, 34]. Figure 9b demonstrates the ν_1 and ν_2 modes with the best fitting results using Gauss function. Based on the model proposed by Jehng [35], the ν_1 mode can be assigned to the symmetric stretching mode of the NbO_6 octahedra, which corresponds to slightly different Nb–O bond distances. Consequently, the ν_1 mode is sensitive to the change of composition as well as phase structure. For the Bi_2O_3 -modified KNSNT ceramics, the ν_1 mode shifts to a lower frequency with the increase of Bi_2O_3 content (Fig. 9c), due to the reduced distortion of NbO_6 octahedron, thus increasing the crystal symmetry of the ceramics. Furthermore, the degree of relaxor dispersion can be manifested

Fig. 7 Temperature dependences of dielectric permittivity ϵ' and dielectric loss $\tan \delta$ for the KNSNT-10x ceramics. **a** KNN, **b** $x = 0$, **c** $x = 1.0$, and **d** $x = 2.0$

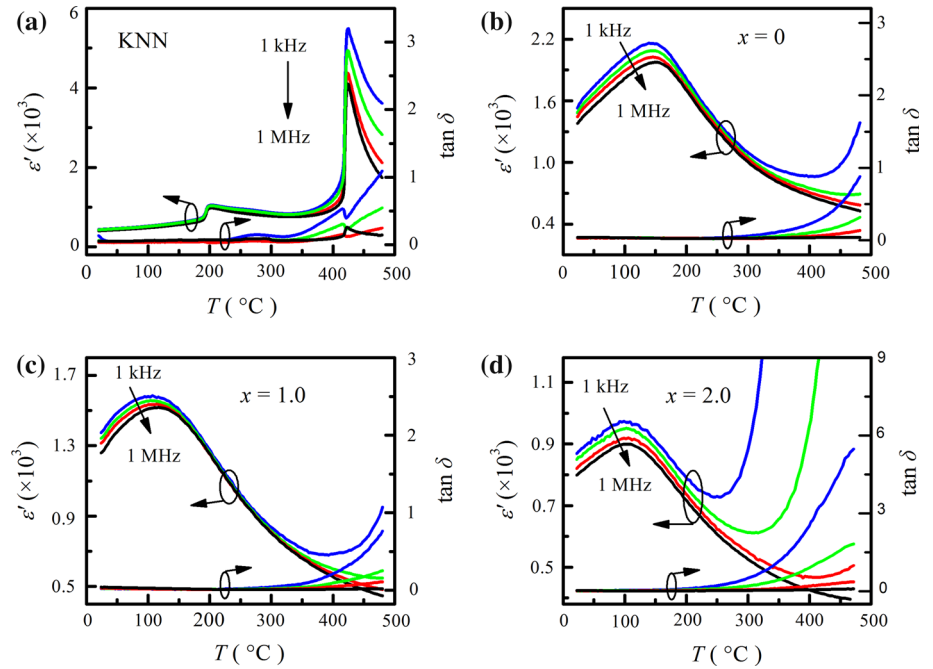


Table 2 Dielectric permittivity ϵ' at 300 K, the maximum dielectric permittivity ϵ'_m , Curie temperature T_m , diffusion coefficient γ , and field-induced strains S_{33} of the KNSNT-10x ceramics

Sample	ϵ'	ϵ'_m	T_m (°C)	γ	S_{33} ($\times 10^{-3}$)
KNN	427	4376	428	1.08	–
$x = 0$	1583	2088	148	1.97	0.79
$x = 0.5$	1465	1854	121	1.98	0.66
$x = 1.0$	1310	1555	109	2.0	0.33
$x = 1.5$	932	1071	105	1.95	0.20
$x = 2.0$	828	918	102	1.92	0.13

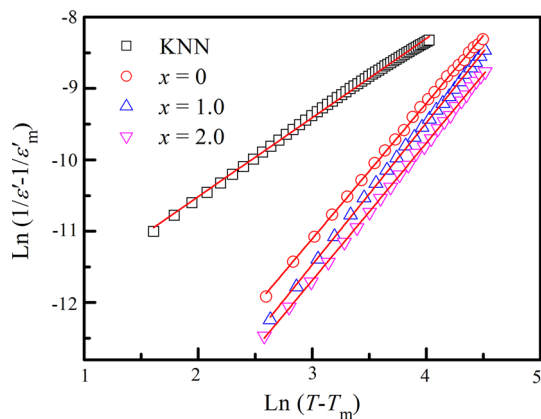


Fig. 8 $\ln(1/\epsilon' - 1/\epsilon'_m)$ as a function of $\ln(T - T_m)$ for the KNSNT-10x ceramics (the symbols experimental data, the solid lines fitting by the modified Curie–Weiss law)

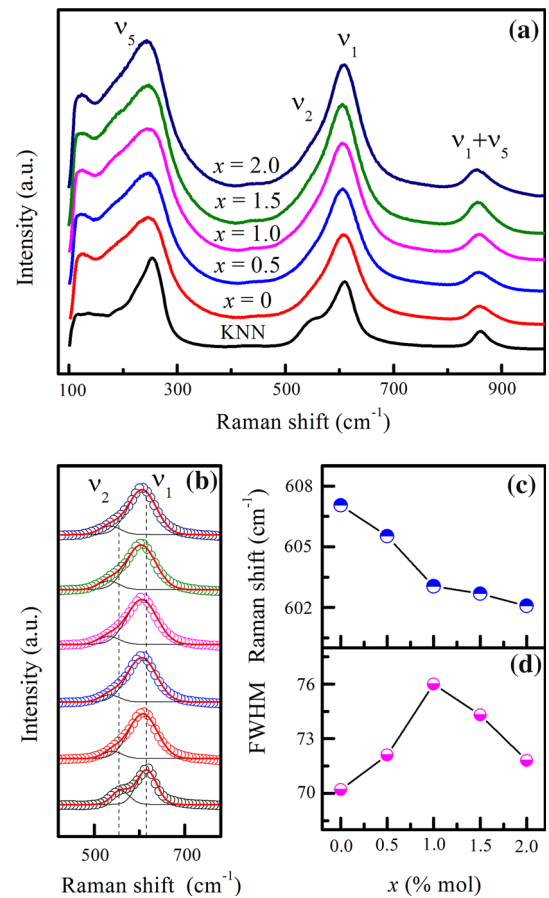


Fig. 9 **a** Raman spectra of the KNSNT-10x ceramics, **b** the ν_1 and ν_2 modes fitting by Gauss function, **c** Raman shift of ν_1 mode as a function of x content, and **d** FWHM of ν_1 mode as a function of x content

Fig. 10 **a** Ferroelectric hysteresis (P – E) loop and **b** strain (S_{33}) versus electric field (E) of the KNSNT-10 x ceramics (along the *arrow* $x = 0, 0.5, 1.0,$ and $2.0,$ respectively)

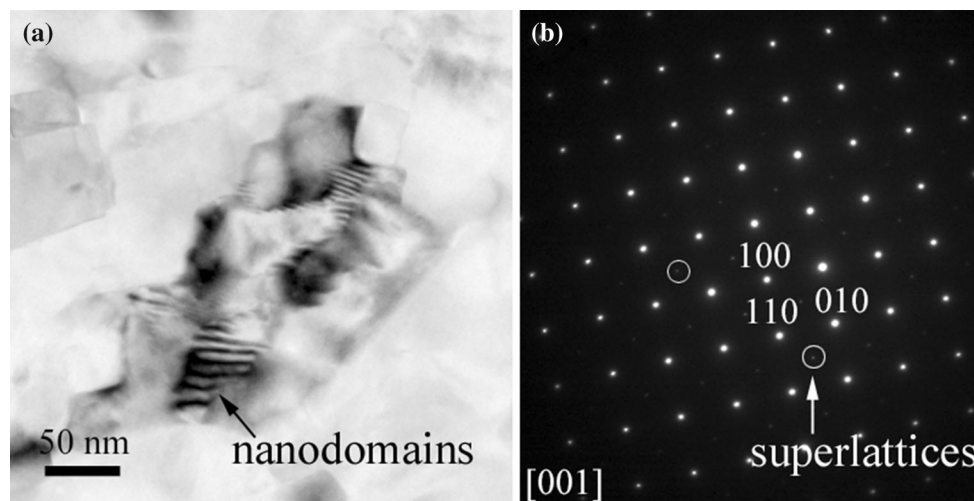
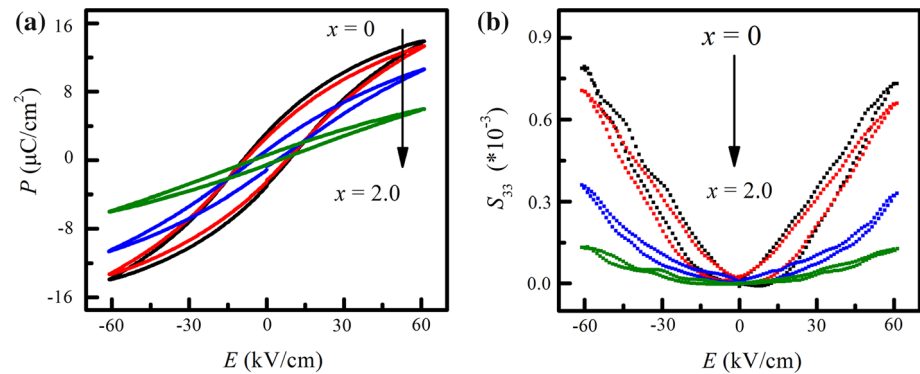


Fig. 11 **a** Bright-field TEM image and **b** SAED pattern along the [001] zone axis of the KNSNT-10 ceramic

by the full width at half maximum (FWHM) of ν_1 mode [21]. Figure 9d shows the FWHM of ν_1 mode as a function of x content. As the content of Bi_2O_3 is increased from 0 to 1.0, the ν_1 mode becomes broader. As a result, the degree of relaxor dispersion of the KNSNT-10 x ceramics is increased. For the relaxor KNSNT-10 ferroelectric, the reduction of long-range ordering structure makes the light scattering to be reduced and thus the optical transparency is increased [1].

Ferroelectric hysteresis loops (P – E) of the ceramics are plotted in Fig. 10a. For the KNSNT-10 x ceramic, the value of remnant polarization is significantly lower than the saturation polarization at high electric field, indicating that there is a strong relaxation of polarization in the ceramics. Besides, various electric field P – E loops of the $x = 0$ and $x = 1.0$ ceramics (Fig. S2 in electronic supplementary material) also indicate a typical characteristic for relaxor ferroelectrics [9]. It is noted that the remnant polarization drops gradually as the x content increases from 0 to 2.0 (Fig. 10a), implying that the increase of Bi_2O_3 addition can degrade ferroelectric properties of the KNSNT ceramics. Figure 10b shows bipolar field-induced strains of the KNSNT-10 x ceramics. A

butterfly-type strain curve is observed for $x = 0$, and the strain value is 0.079 % at 60 kV/cm (Table 2). With the Bi_2O_3 content increasing to $x = 1.0$, the strain value decreases to 0.033 %. For ferroelectric ceramics, EO property originates from the microdomain movement under applied electric field [1, 9]. The measured linear EO coefficients can be related to the spontaneous polarization as follows [36, 37]:

$$r_c = 2\varepsilon_0\varepsilon'g_cP_s, \quad (6)$$

where ε_0 is the vacuum permittivity, ε' is the dielectric permittivity, and g_c is the polarization-related quadratic EO coefficient. From the equation, the changes of EO coefficient r_c should be related to the dielectric constant and spontaneous polarization. Indeed, as the content of Bi_2O_3 is increased, both spontaneous polarization P_s and dielectric permittivity ε' decrease (Table 2). As a result, the EO response of the KNSNT-10 x ceramics is weakened.

Figure 11 displays TEM image and selected area electron diffraction (SAED) pattern from the same area with a representative feature of the KNSNT-10 ceramic. In Fig. 11a, fingerprint morphology nanodomains with length

shorter than 50 nm are clearly visible. According to the classical theory of ferroelectric domains, the domain wall can be considered as the layer that separates two domains with different but crystallographically equivalent directions of the polarization vector, and the domain wall energy is proportional to the squared value of the domain size. Therefore, the nanodomain wall energy is inherently lower in such nanodomains of the KNSNT-10 ceramic. As a result, the nanodomain can be easily reoriented under electric fields [38, 39]. Ultimately, a high EO response is obtained for the KNSNT-10 ceramic (26.1 pm/V). Figure 11b shows the SAED pattern along the [100] zone axis, in which superlattice reflections are observed (marked by rings). From the fundamental perovskite reflections, these superlattice reflections originate from slight deviations of the ideal perovskite structure [40]. Combining with the results of Raman spectra (Fig. 9c), it is believed that the superlattice reflection dominates from the NbO₆ oxygen octahedral tilting in the relaxor ferroelectric.

Conclusions

Lead-free transparent electro-optical KNSNT-10x ceramics ($x = 0-2.0$) have been fabricated using the conventional solid-state reaction route. The phase structure of the ceramics presented cubic-like symmetry with the addition of Bi₂O₃, and their average grain size decreased with the increasing Bi₂O₃ concentration. As a result, optical anisotropy and birefringence of light of the grains were greatly reduced; a high transparency of 51.5 % at 633 nm wavelength was obtained for KNSNT-10 transparent ceramics. In addition, with increasing Bi₂O₃ concentration ($x \leq 1.0$), the KNSNT ceramics became more relaxor like. For the KNSNT-10 ceramics, fingerprint morphological nanodomains with the length shorter than 50 nm were observed, which may be sensitive to electric field. Finally, a large effective linear electro-optical coefficient of 26.1 pm/V was obtained for the KNSNT-10 ceramics.

Acknowledgements This work was supported by the National Natural Science Foundation (51172187), the SPDRF (20116102130002, 20116102120016) and 111 Program (B08040) of MOE, and Xi'an Science and Technology Foundation (CX12174, XBCL-1-08), the Shaanxi Province Science Foundation (2013KW12-02), the SKLP Foundation (KP201421), and the Fundamental Research Funds for the Central Universities (3102014JGY01004) of China.

References

- Haertling GH (1987) PLZT electrooptic materials and applications: a review. *Ferroelectrics* 75:25–55
- Uchino K (1995) Electro-optic ceramics and their display applications. *Ceram Int* 21:309–315
- Sternberg A (1989) Transparent ferroelectric ceramics: properties and applications. *Ferroelectrics* 91:53–67
- Aillierie M, Fontana MD, Abdi F, Carabatos-Nedelec C, Theofanous N, Alexakis G (1989) Influence of the temperature-dependent spontaneous birefringence in the electro-optic measurements of LiNbO₃. *J Appl Phys* 65:2406–2408
- Qian XS, Wu H, Wang Q, Yu ZY, Xu F, Lu YQ, Chen YF (2011) Electro-optic tunable optical isolator in periodically poled LiNbO₃. *J Appl Phys* 109(5):053111
- Haertling GH, Land CE (1971) Hot-pressed (Pb, La)(Zr, Ti)O₃ ferroelectric ceramics for electrooptic applications. *J Am Ceram Soc* 54:1–11
- He C, Chen H, Sun L, Sun L, Wang J, Xu F, Du C, Zhu K, Liu Y (2012) Effective electro-optic coefficient of (1 - x)Pb(Zn_{1/3}Nb_{2/3})O₃ - xPbTiO₃ single crystals. *Cryst Res Technol* 47(6):610–614
- Ruan W, Li G, Zeng J, Bian J, Kamzina LS, Zeng H, Zheng L, Ding A (2010) Large electro-optic effect in La-doped 0.75Pb(Mg_{1/3}Nb_{2/3})O₃-0.25PbTiO₃ transparent ceramic by two-stage sintering. *J Am Ceram Soc* 93(8):2128–2131
- Ruan W, Li G, Zeng J, Kamzina LS, Zeng H, Zhao K, Zheng L, Ding A (2011) Origin of the giant electro-optic Kerr effect in La-doped 75PMN-25PT transparent ceramics. *J Appl Phys* 110(7):074109
- Withers RL, Liu Y, Welberry TR (2009) Structured diffuse scattering and the fundamental 1-d dipolar unit in PLZT (Pb_{1-y}La_y)_{1-a}(Zr_{1-x}Ti_x)_{1-b}O₃ (7.5/65/35 and 7.0/60/40) transparent ferroelectric ceramics. *J Solid State Chem* 182:348–355
- Iamsasri T, Tutuncu G, Uthaisar C, Pojprapai S, Jones JL (2013) Analysis methods for characterizing ferroelectric/ferroelastic domain reorientation in orthorhombic perovskite materials and application to Li-doped Na_{0.5}K_{0.5}NbO₃. *J Mater Sci* 48:6905–6910. doi:10.1007/s10853-013-7495-2
- Cheng H, Zhou W, Du H, Luo F, Zhu D, Xu B (2014) Effect of sintering temperature on phase structure, microstructure, and electrical properties of (K_{0.5}Na_{0.5})NbO₃-(Ba_{0.6}Sr_{0.4})_{0.7}Bi_{0.2}TiO₃ lead-free ceramics. *J Mater Sci* 49:1824–1831. doi:10.1007/s10853-013-7870-z
- Sun X, Chen J, Yu R, Sun C, Liu G, Xing X, Qiao L (2009) BiScO₃ doped (Na_{0.5}K_{0.5})NbO₃ lead-free piezoelectric ceramics. *J Am Ceram Soc* 92(1):130–132
- Gaur R, Singh KC, Laishram R (2013) Structural and piezoelectric properties of barium-modified lead-free (K_{0.45}Li_{0.045}Na_{0.5})(Nb_{0.9}Ta_{0.1})O₃ ceramics. *J Mater Sci* 48:5607–5613. doi:10.1007/s10853-013-7355-0
- Li H, Gong D, Yang W, Zhou Z (2013) Microstructure and piezoelectric properties of NaF-doped K_{0.5}Na_{0.5}Nb_{0.95}Ta_{0.05}O₃ lead-free ceramics. *J Mater Sci* 48:1396–1400. doi:10.1007/s10853-012-6887-z
- Zhou JJ, Li JF, Zhang XW (2012) BiFeO₃-modified (Li, K, Na)(Nb, Ta)O₃ lead-free piezoelectric ceramics with temperature-stable piezoelectric property and enhanced mechanical strength. *J Mater Sci* 47:1767–1773. doi:10.1007/s10853-011-5957-y
- Kosec M, Bobnar V, Hrovat M, Bernard J, Malic B, Holc J (2004) New lead-free relaxors based on the K_{0.5}Na_{0.5}NbO₃-SrTiO₃ solid solution. *J Mater Res* 19(6):1849–1854
- Kroupa J, Petzelt J, Malic B, Kosec M (2005) Electro-optic properties of KNN-STO lead-free ceramics. *J Phys D Appl Phys* 38:679–681
- Li F, Kwok KW (2013) Fabrication of transparent electro-optic (K_{0.5}Na_{0.5})_{1-x}Li_xNb_{1-x}Bi_xO₃ lead-free ceramics. *J Eur Ceram Soc* 33:123–130
- Li K, Li FL, Wang Y, Kwok KW, Chan HLW (2011) Hot-pressed K_{0.48}Na_{0.52}Nb_{1-x}Bi_xO₃ ($x = 0.05-0.15$) lead-free ceramics for electro-optic applications. *Mater Chem Phys* 131:320–324
- Guo Y, Kakimoto K, Ohsato H (2004) Ferroelectric-relaxor behavior of (Na_{0.5}K_{0.5})NbO₃-based ceramics. *J Phys Chem Sol* 65:1831–1835

22. Liu Z, Fan H, Long C (2014) Dielectric nonlinearity and electrical properties of $K_{0.5}Na_{0.5}NbO_3$ - $SrTiO_3$ relaxor ferroelectrics. *J Mater Sci* 49:8107–8115. doi:10.1007/s10853-014-8518-3
23. Wan X, Wang DY, Zhao X, Luo H, Chan HLW, Choy CL (2005) Electro-optic characterization of tetragonal $(1-x)Pb(Mg_{1/3}Nb_{2/3})O_3$ - $xPbTiO_3$ single crystals by a modified Sénarmont setup. *Solid State Commun* 134:547–551
24. Peelen JGJ, Metselaar R (1974) Light scattering by pores in polycrystalline materials: transmission properties of alumina. *J Appl Phys* 45:216–220
25. Zuo R, Fang X, Chun Y (2007) Phase structures and electrical properties of new lead-free $(Na_{0.5}K_{0.5})NbO_3$ - $(Bi_{0.5}Na_{0.5})TiO_3$ ceramics. *Appl Phys Lett* 90(9):092904
26. Wang XX, Tang XG, Kwok KW, Chan HLW, Choy CL (2005) Effect of excess Bi_2O_3 on the electrical properties and microstructure of $(Bi_{1/2}Na_{1/2})TiO_3$ ceramics. *Appl Phys A* 80: 1071–1075
27. Du H, Liu D, Tang F, Zhu D, Zhou W, Qu S (2007) Microstructure, piezoelectric, and ferroelectric properties of Bi_2O_3 -added $(K_{0.5}Na_{0.5})NbO_3$ lead-free ceramics. *J Am Ceram Soc* 90(9):2824–2829
28. Wang SF, Zhang J, Luo DW, Gu F, Tang DY, Dong ZL, Tan GEB, Que WX, Zhang TS, Li S, Kong LB (2013) Transparent ceramics: processing, materials and applications. *Prog Solid State Chem* 41:20–54
29. Anselmi-Tamburini U, Woolman JN, Munir ZA (2007) Transparent nanometric cubic and tetragonal zirconia obtained by high-pressure pulsed electric current sintering. *Adv Funct Mater* 17:3267–3273
30. Pauling L (1929) The principles determining the structure of complex ionic crystals. *J Am Chem Soc* 51:1010–1026
31. Uchino K, Nomura S (1982) Critical exponents of the dielectric constants in diffused phase transition crystals. *Ferroelectr Lett* 44:55–61
32. Wei X, Feng Y, Yao X (2003) Dielectric relaxation behavior in barium stannate titanate ferroelectric ceramics with diffused phase transition. *Appl Phys Lett* 83:2031–2033
33. Burton BP, Cockayne E, Waghmare UV (2005) Correlations between nanoscale chemical and polar order in relaxor ferroelectrics and the length scale for polar nanoregions. *Phys Rev B* 72(6):064113
34. Tan X, Fan H, Ke S, Zhou L, Mai YW, Huang H (2012) Structural dependence of piezoelectric, dielectric and ferroelectric properties of $K_{0.5}Na_{0.5}(Nb_{1-2x/5}Cu_x)O_3$ lead-free ceramics with high Q_m . *Mater Res Bull* 47:4472–4477
35. Jehng JM, Wachs IE (1991) Structural chemistry and raman spectra of niobium oxides. *Chem Mater* 3:100–107
36. Wan X, Luo H, Zhao X, Wang DY, Chan HLW, Choy CL (2004) Refractive indices and linear electro-optic properties of $(1-x)Pb(Mg_{1/3}Nb_{2/3})O_3$ - $xPbTiO_3$ single crystals. *Appl Phys Lett* 85:5233–5235
37. Fontana MD, Abdi F, Wojcik K (1995) Electrooptical properties of a single domain $PbTiO_3$ crystal. *J Appl Phys* 77:2102–2106
38. Fu J, Zuo R, Xu Z (2011) High piezoelectric activity in $(Na, K)NbO_3$ based lead-free piezoelectric ceramics: contribution of nanodomains. *Appl Phys Lett* 99(6):062901
39. Sato Y, Hirayama T, Ikuhara Y (2012) Evolution of nanodomains under DC electrical bias in $Pb(Mg_{1/3}Nb_{2/3})O_3$ - $PbTiO_3$: an in-situ transmission electron microscopy study. *Appl Phys Lett* 100(17):172902
40. Woodward DI, Reaney IM (2005) Electron diffraction of tilted perovskites. *Acta Cryst B* 61:387–399